Modeling and simulation of a 2-DOF bidirectional electrothermal microactuator

N. Topaloglu, C. Elbuken, P. M. Nieva*, M. Yavuz, J. P. Huissoon
Dept. of Mechanical & Mechatronics Eng., University of Waterloo
200 University Ave. West, Waterloo, ON Canada N2L3G1

ABSTRACT

In this paper we present the modeling and simulation of a 2 degree-of-freedom (DOF) bidirectional electrothermal actuator. The four arm microactuator was designed to move in both the horizontal and vertical axes. By tailoring the geometrical parameters of the design, the in-plane and out-of-plane motions were decoupled, resulting in enhanced mobility in both directions. The motion of the actuator was modeled analytically using an electro-thermo-mechanical analysis. To validate the analytical model, finite element simulations were performed using ANSYS. The microactuators were fabricated using PolyMUMPS process and experimental results show good agreement with both the analytical model and the simulations. We demonstrated that the 2-DOF bidirectional electrothermal actuator can achieve 3.7 μm in-plane and 13.3 μm out-of-plane deflections with an input voltage of 10 V.

Keywords: MEMS, 2-DOF microactuator, bidirectional microactuator, electrothermal microactuator

1. INTRODUCTION

MEMS (Micro Electro Mechanical Systems) based microactuators can be operated using electrothermal, electrostatic, piezoelectric, magnetic and pneumatic actuation mechanisms. Electrothermal actuation is commonly used in MEMS since it features high deflections with relatively low voltage levels. Compared to other actuation schemes, electrothermal microactuators deliver larger forces and demonstrate high repeatability.

One of the most important design constraints in electrothermal actuators is the range of motion. Since the introduction of the electrothermal actuator by Guckel et al.[1], many studies have been done to improve their deflection range. However, the majority of these actuators are limited to operate in one dimension[2-4] (either in-plane or out-of-plane) and are simply unidirectional, i.e. they can only move in one direction. Recently, one degree-of-freedom (1-DOF) bidirectional actuators have also been introduced[5, 6]. However, a higher degree-of-freedom is crucial to the operation of microactuators since it enables the actuator to be used for a broader range of applications. Some other studies in the literature have reported 2-DOF microactuators which can achieve both in-plane and out-of-plane deflections[7, 8]. Although these actuators cleverly combine different actuation schemes to move the actuators in two axes, they have significant drawbacks. For instance, the actuator reported by Liao et al.[7] requires very high voltages, since it uses electrostatic actuation for out-of-plane motion. The actuator reported by Wu et al.[8] suffers from difficulties in fabrication of large fixed-free structures that use bimorph actuation.

This paper introduces a 2-DOF bidirectional electrothermal actuator for the first time. To the best of the authors' knowledge, a 2-DOF bidirectional electrothermal actuator has not been reported before. The actuator can move in all four orthogonal directions of the Cartesian plane. Modeling of the microactuator was performed using on electro-thermo-mechanical analysis. Finite element simulations were used to verify the validity of the analytical model. The actuators have been fabricated using PolyMUMPs®, thus they are compatible with standard microfabrication technologies. Experiments show that the fabricated microactuators are indeed capable of achieving the in-plane and out-of-plane deflections predicted by the models.

*pnieva@uwaterloo.ca; simslab.uwaterloo.ca

Modeling, Signal Processing, and Control for Smart Structures 2008, edited by Douglas K. Lindner
Proc. of SPIE Vol. 6926, 692605, (2008) · 0277-786X/08/$18 · doi: 10.1117/12.776594

2. ANALYTICAL MODEL

2.1 Design considerations

The 2-DOF bidirectional microactuator is composed of four thin arms and a shuttle. The Scanning Electron Microscope (SEM) micrograph of the actuator is shown in Figure 1. The arms are 200 µm long. A Vernier scale with 2 µm wide fingers was used to facilitate the deflection measurements. The width of the arms and the spacing between the arms vary according to the amount of deflection that needs to be achieved. The core of the design is that the inner and outer arms lie at different heights, with the outer arms positioned at a higher level. Each one of the four arms is connected to different contact pads, so that voltage can be applied to two of the arms selectively depending on the desired deflection.

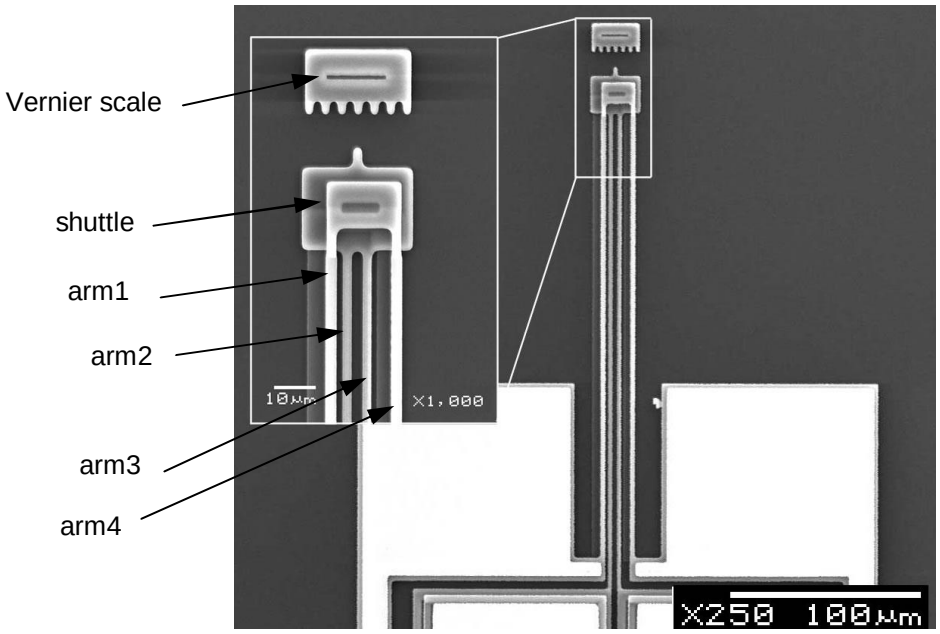

Figure 1. SEM micrograph of the four arm microactuator. The inset shows the magnified view of the tip with the Vernier scale.

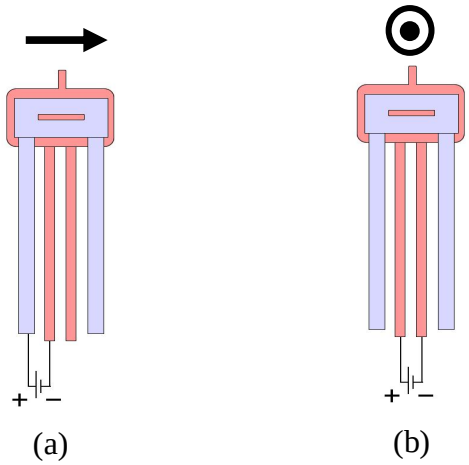

Figure 2. Schematic diagram of a 2-DOF bidirectional microactuator operating in the (a) in-plane (towards the right), and the (b) out-of-plane deflection modes (upward)

The operation of the microactuator in two particular modes is shown schematically in Figure 2. Figure 2a shows the setup used to achieve an in-plane deflection towards the right. In this case, a potential difference is applied between arms1 and 2 (see Figure 1). This generates a current flow between the two arms, thus increasing the temperature of the arms by joule heating. The increment in length of the arms due to the thermal expansion causes an arching motion of the tip and deflects the actuator towards the right. This type of actuation mechanism was first by Guckel et al using a two arm microactuator with different arm widths[1]. Similarly, to move the four-arm microactuator towards the left, voltage is applied to arms 3 and 4. Figure 2b shows the setup used to achieve an upward out-of-plane deflection. In this case, the inner arms (arms 2 and 3) are heated. Since the inner arms are connected to the shuttle at a lower level than the outer arms, their expansion pushes the shuttle upwards. Similarly, to move the four-arm microactuator downward, voltage is applied to arms 1 and 4.

This four-arm microactuator was designed to be compatible with the Polysilicon Multi-user MEMS Process (PolyMUMPs®) offered by MEMSCAP. The inner arms are formed using the first polysilicon layer that has a thickness of 2 µm. A sacrificial layer of phosphosilicate glass (PSG) is then deposited. The outer arms are formed by patterning the second polysilicon layer deposited on the PSG. This way, the inner arms and outer arms are fabricated at different heights.

2.2 Electro-thermal-mechanical model

The analytical model of the 2-DOF bi-directional actuator presented in this work involves two parts. The first part is the determination of the temperature distribution and the second part is the calculation of the deflection using the temperature distribution of the arms.

A 1-D schematic diagram of the four-arm microactuator is depicted in Figure 3. Since the arms are narrow, thin and long, it can be assumed that the heat flows only in one direction. Two of the pads are biased with constant voltage. An electrical current passes through two of the arms depending of the mode of actuation. For the remaining of this paper, we will call these two arms the “hot arms”. The remaining two arms will be called the “cold arms.”

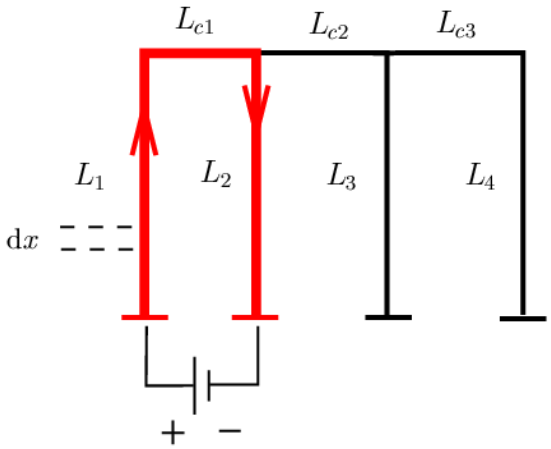

Figure 3. Simplified schematic diagram of the four-arm microactuator showing the one-dimensional (1-D) current flow.

The heat generation in an infinitesimal portion of length “dx” on a hot arm “i”can be expressed as:

$$g_i = \left(\frac{V_i dx}{L_i}\right)^2 \frac{1}{\rho\left(dx/A\right)}, \tag{1}$$

where ρ is the resistivity, A is the cross-sectional area and V_i is the voltage across hot arm i, which can be written using voltage division

$$V_i = \frac{R_i}{R_1 + R_2 + R_{c1}} V \,. \tag{2}$$

The steady-state heat equation for a hot arm can then be written as:

$$k_i \frac{\partial T_i}{\partial x} A = \frac{S_i \left(T_i \left(x \right) - T_s \right)}{Z_i t_i} A dx - g_i \,. \tag{3}$$

In the above equation, the first term in the right-hand side presents the heat loss to the substrate through the air gap and the nitride layer. Z_i is the summation of thermal resistances of the air gap and nitride layer, expressed as:

$$Z_i = \frac{t_a}{k_a} + \frac{t_n}{k_n} \tag{4}$$

In Equation (4), t_a and t_n are the thicknesses of air and nitride layers, respectively, whereas k_a and k_n are the thermal conductivities of air and nitride, respectively. The heat flow to the substrate through the air gap is radial. To account for the spreading of the heat flux lines as the heat flows through the air gap to the substrate, the dimensionless shape factor S_i is used [9]:

$$S_i = \frac{t_i}{w_i} \left(2 \frac{t_a}{t_i} + 1 \right) + 1 \,. \tag{5}$$

Rearranging terms, Equation (3) can be rewritten as

$$\frac{d^2 T_i \left(x \right)}{dx^2} = A_i \left(T_i \left(x \right) - T_s \right) - B_i \,, \tag{6}$$

where,

$$A_i = \left(\frac{S_i}{k_p Z_i t} \right)^{1/2} \text{ and } B_i = \frac{V_i^2}{L_i^2 \rho k_p} \,. \tag{7}$$

For the cold arms, the heat equation is very similar to Equation (3) except that there is no heat generation:

$$\frac{d^2 T_j \left(x \right)}{dx^2} = A_j \left(T_j \left(x \right) - T_s \right) . \tag{8}$$

Note that in Equation (8), "j" is used as an index for the cold arms and "i" is used as an index for the hot arms. The solution of the differential equations (3) and (8) is given by

$$T_i \left(x \right) = T_s + \frac{B_i}{A_i^2} + K_{i1} e^{A_i x} + K_{i2} e^{-A_i x} \text{ and } T_j \left(x \right) = T_s + K_{j1} e^{A_j x} + K_{j2} e^{-A_j x} \,. \tag{9}$$

To find the temperature distributions, eight unknowns (K_{i1}, K_{i2}, K_{j1} and K_{j2}, $i = 1,2$ and $j = 3,4$) need to be determined. The first four boundary conditions are the temperatures at the anchor of each arm:

$$T_i\left(0\right) = T_s \text{ and } T_j\left(0\right) = T_s, \tag{10}$$

Three other boundary conditions are obtained by assuming that the temperature at the tip of the arms (i.e. the temperature at the shuttle) is equal to the substrate temperature

$$T_i\left(L_i\right) = T_{shuttle} \text{ and } T_j\left(L_j\right) = T_{shuttle}. \tag{11}$$

To find the temperature at the shuttle, $T_{shuttle}$, the final boundary condition is defined by the continuity of heat flux as

$$-k_p w_1 t_1 \left(\frac{dT_1}{dx}\right)_{x=L_1+L_{c1}} - k_p w_2 t_2 \left(\frac{dT_2}{dx}\right)_{x=L_2} = \frac{\left(T_{shuttle} - T_s\right) k_p w_3 t_3}{L_3} + \frac{\left(T_{shuttle} - T_s\right) k_p w_4 t_4}{L_4} \tag{12}$$

The left-hand side of equation (12) represents the heat flow from the hot arms and the right-hand side corresponds to the heat flowing to the cold arms.

Based on the temperature distributions, $T_i\left(x\right)$, the deflection at the tip can be found by thermo-mechanical analysis. The thermal expansion of arm *i* can be found as

$$\Delta L_i = \alpha \int_0^{L_i} \left(T_i\left(x\right) - T_s\right) dx, \tag{13}$$

where α is the coefficient of thermal expansion (CTE).

A structural analysis is performed to determine the deflection at the tip. The actuator is a statically indeterminate system with a degree of indeterminacy of nine. To solve the indeterminacy, we have used the force method[10]. In this method three of the four arms are released from their supports (refer to Figure 4) generating different reaction forces and moments, X_i, that satisfy the boundary conditions. To find the reaction forces and moments, the flexibility matrix of the structure is determined from the geometry of the four-arm structure and mechanical properties of the polysilicon layer.

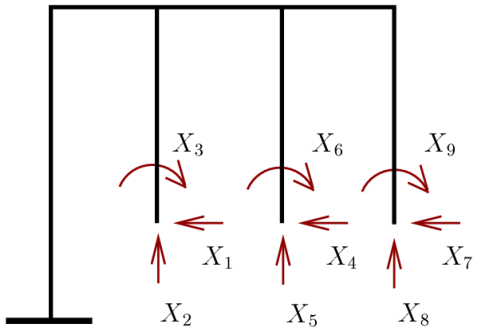

Figure 4. Free body diagram of the four-arm actuator showing the reaction forces and moments.

Once X_i ($i = 1,\ldots,9$) is calculated, the horizontal deflection of the tip is found to be

$$u = \frac{1}{EI_2}\left[\frac{L_1^3}{6}\left(X_1 + X_4 + X_7\right) + \frac{L_1^2}{2}\left(H_1 + H_2 + H_3\right)\right], \tag{14}$$

where

$$\begin{aligned} H_1 &= X_1\left(L_2 - L_1\right) - X_2 L_{c1} - X_3 \\ H_2 &= X_4\left(L_3 - L_1\right) - X_5\left(L_{c1} + L_{c2}\right) - X_6 \\ H_3 &= X_7\left(L_4 - L_1\right) - X_8\left(L_{c1} + L_{c2} + L_{c3}\right) - X_9 \end{aligned} \tag{15}$$

Since the thermal-mechanical model for the horizontal and vertical deflection is similar, the same procedure can be applied to find the vertical deflection. However, the flexibility matrix and the reaction forces and moments need to be reformulated.

3. FINITE ELEMENT MODELING

Finite element simulations of the 2-DOF bidirectional microactuator were performed using ANSYS® by following the sequential modeling approach. For the simulations, the temperature and mechanical physics environments were defined separately using the 3D model elements SOLID98 and SOLID92, respectively. The temperature physics environment is simulated first to obtain the temperature profile along the actuator as a function of the input voltage. The ends the arms connected to the substrate were kept at a constant temperature since it is assumed that the substrate behaves as a heat sink. A convective heat loss coefficient was defined for all surfaces of the arms. Hence, heat convection from the sides was also taken in to account. The result of the temperature environment analysis is then used as and input for the mechanical deformation analysis. For the mechanical environment, the arms were assumed to be fixed at the anchors. The mechanical deformation environment calculates the thermal expansion and the resultant deflection of the actuator using the temperature distribution obtained from temperature environment. The same meshing was used for both environments. The actuator was modeled with approximately 16,300 elements. It was observed that the sequential analysis is much more computationally efficient than a coupled analysis which handles thermal and mechanical analyses in a single physics environment. The material properties used in the simulations are listed in Table 1. These values are specified by the PolyMUMPs® process.

Table 1. Material properties used in this paper

Material property [11]	Value	Unit
Young's modulus of polySi	162×10^9	Pa
Poisson's ratio	0.22	-
Thermal conductivity of polySi	41×10^{-6}	W μm^{-1} C^{-1}
Thermal conductivity of nitride	2.25×10^{-6}	W μm^{-1} C^{-1}
Thermal conductivity of air	0.026×10^{-6}	W μm^{-1} C^{-1}
Thermal coefficient of expansion	3.5×10^{-6}	C^{-1}
Convection coefficient	$10\text{-}25 \times 10^{12}$	W μm^{-1} C^{-1}
Electrical resistivity of Poly1	20	Ω μm
Electrical resistivity of Poly2	30	Ω μm

The simulations were carried out for both in-plane and out-of-plane motion. Results for the in-plane motion (towards the right) and out-of-plane motion (upwards) are presented in Figure 5 and Figure 6, respectively. Figure 5 shows the

temperature distribution along the device when an input voltage of around 8 V is applied to arms 1 and 2. The inset in this figure shows the deflected shape and the original un-deformed shape. From the figure, it can be seen that the in-plane deflection is approximately 2.5 µm (see DMX value on the upper-left corner of figure 5). Also, note that the temperature reaches a maximum of 1030 K along arms1 and 2. Similarly, Figure 6 shows the temperature distribution along the device when an input voltage of around 8 V is applied to arms 2 and 3. Once again, the inset in the figure shows the deflected shape and the original un-deformed shape. Results show that the out-of-plane deflection is approximately 10 µm and the maximum temperature reached by the arms is around 898 K. Similar results were obtained for the in-plane motion and the out-of-plane motion in the opposite directions.

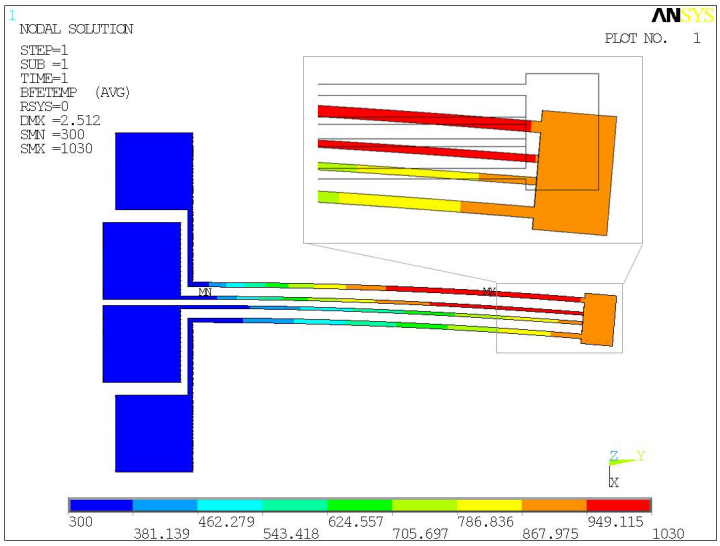

Figure 5. Finite element simulations showing the temperature profile and tip deflection during in-plane motion (towards the right) of the 2-DOF bidirectional microactuator for an input voltage of 8 V applied to arms 1 and 2.

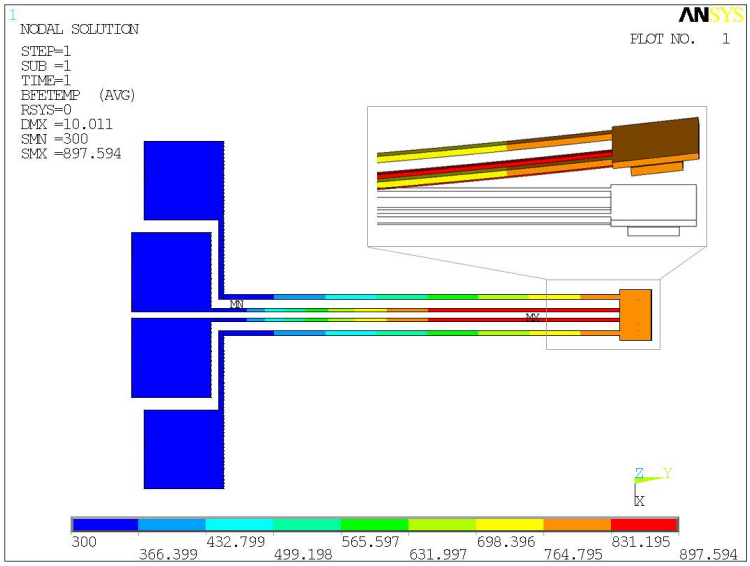

Figure 6. Finite element simulations showing the temperature profile and tip deflection during out-of-plane motion (upwards) of the 2-DOF bidirectional microactuator for an input voltage of 8 V applied to arms 2 and 3.

4. EXPERIMENTS AND DISCUSSION

The 2-DOF bi-directional microactuators were fabricated using PolyMUMPs run 78. PolyMUMPs is a three-layer polysilicon MEMS surface micromachining process[11] that uses a 600 nm LPCVD (low pressure chemical vapor deposition) silicon nitride film as isolation. The 2.0 µm thick first polysilicon structural layer (Poly1) was deposited and patterned to form the inner arms (2 and 3). The 2.0 µm thick PSG (phosphosilicate glass) sacrificial layer (Oxide1) was patterned and etched to form the anchors of inner arms. The second 0.75 µm thick PSG sacrificial layer (Oxide2) forms the vertical air-gap between the inner and outer arms. This layer was patterned using the poly1-poly2-via mask to form the connection between the inner and the outer arms on the shuttle. The outer arms (1 and 4) are made in the PolyMUMPs second structural layer (Poly2), which is 1.5 µm thick. The gap between the outer arms and inner arms is 0.75 µm, which is the thickness of Oxide2 (Figure 7a). Since a thicker gap will result in more moment and deflection in the out-of-plane direction, a 0.5 µm thick Poly0 layer is deposited underneath the outer arms in some designs, in order to elevate the outer arms (Figure 7b). The 0.5 µm thick gold layer is used to form the electrical contacts. Vernier scales were included at the tip of the actuators to facilitate the in-plane measurements.

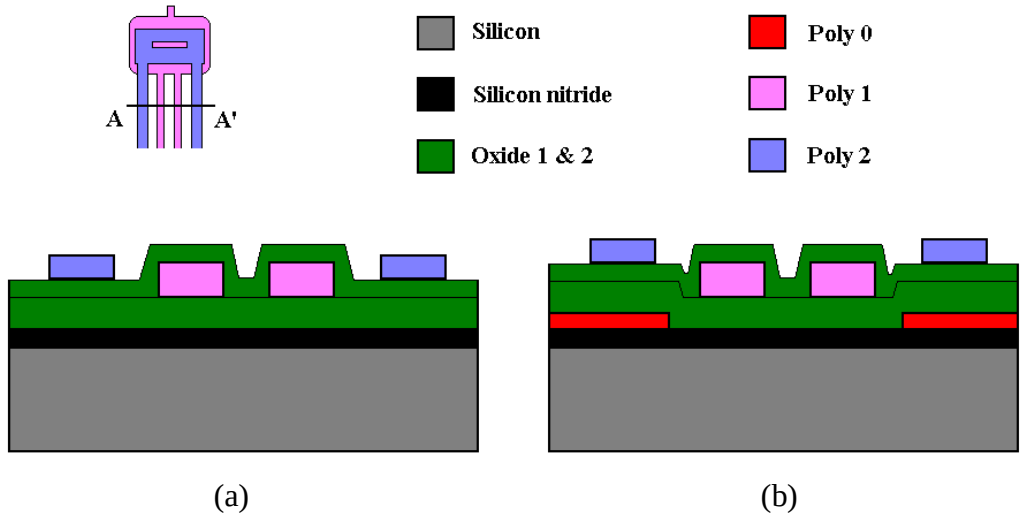

Figure 7. Schematic showing the cross-sectional view of the 2-DOF bi-directional microactuators fabricated using PolyMUMPs run 78 (a) Microactuators without the Poly0 layer and with a total air gap of 0.75 µm between the outer and inner arms (b) Microactuators with the Poly0 layer and with a total air gap of 1.25 µm between the inner and outer arms.

An optical microscope with an integrated CCD camera was used for the in-plane testing. A DC power supply and a pair of DC microprobes were used to apply a voltage to two of the contact pads to deflect the four-arm microactuator either towards the right (arms 1 and 2) or towards the left (arms 3 and 4). The optical images for both four-arm microactuators fabricated without and with the Poly0 layer deflecting towards the right are shown in Figure 8a and 8b, respectively. For the case of the microactuator with a Poly0 layer, an input voltage of 10 V applied to arms 1 and 2 generated a tip deflection of approximately 3.7 µm. The same amount of deflection (~3.7 µm) was observed when a voltage of 10 V was applied to arms 3 and 4, thus generating a motion towards the left. The operation of the four-arm microactuator fabricated without the Poly0 layer was very similar. Although the finite element simulations show some variation in the amount of the in-plane deflection of both types of microactuators, no measurable difference was noticed due to the accuracy of the Vernier scale.

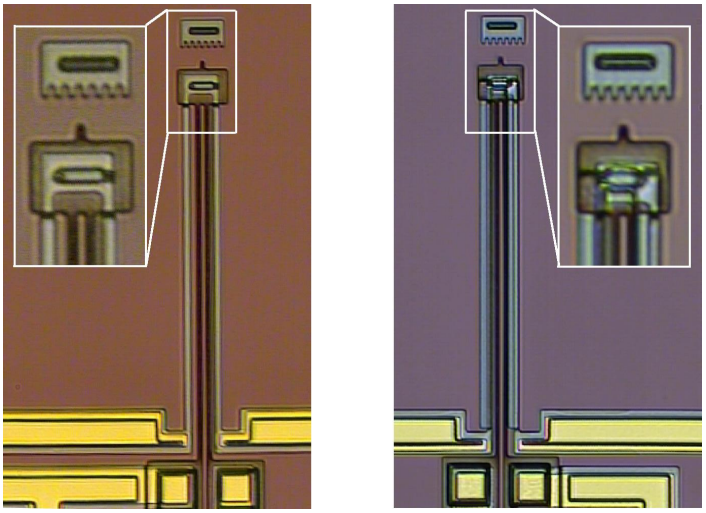

(a) (b)

Figure 8. Optical image of 2-DOF bi-directional microactuators (a) without and (b) with a Poly 0 layer operating in the in-plane mode with an input voltage of 10 V

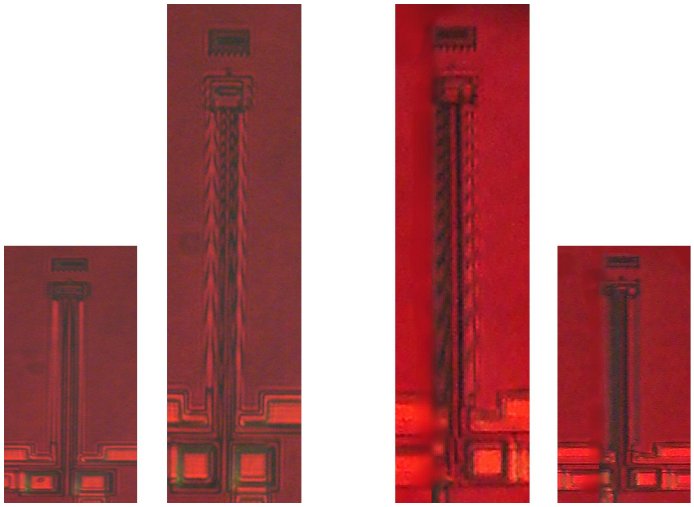

(a) (b)

Figure 9. Optical image of the 2-DOF bi-directional microactuators (a) without and (b) with the Poly 0 layer operating in the out-of-plane mode and generated using laser interferometry. The smaller images show the position of the microactuator at 0 Volts. The larger images show the fringes observed at an input voltage of 10 V.

To measure the ou-of-plane deflection of the 2-DOF bidirectional microactuators, we used laser interferometry. A DC power supply and a pair of DC microprobes were used to apply voltage to two of the contact pads to deflect the four-arm microactuator either upward (arms 2 and 3) or downward (arms 1 and 4). During the measurements, a 633nm Helium Neon laser is focused on the microactuator. Part of the laser beam is reflected back from the polysilicon structural layers, while some of it is reflected back from the silicon nitride layer, deposited on top of the substrate. When no voltage is applied, the air gap between the substrate and the polysilicon arms is quasi-uniform. Note that the uniformity of the air gap depends on the inherent stress gradients of the structural layers and can be easily taken into account if the initial

curling of the microactuator is measured using an optical profilometer. For our case, the stress gradients in the polysilicon structural layers used in the PolyMUMPs process did not cause a significant initial curling. When a potential difference is applied to arms 2 and 3, the microactuator bends up and the thickness of the air gap increases along the length of the beams from the anchor towards the shuttle. This causes interference patterns (fringes) on the actuator surface as a result of the change in the optical path of the laser light across the beam. In this case, a pair of bright and dark fringes corresponds to a height difference of half a wavelength of the laser beam, which is around 0.317 µm. To calculate the deflection, the number of fringes was recorded as the voltage was increased from 1 to 10 Volts with 1 V increments.

Figure 9 shows the fringe patterns obtained for microactuators fabricated without (Figure 9a) and with (Figure 9b) the Poly 0 layer. As can be seen from the figure, the microactuator that was fabricated using the Poly 0 layer presents greater number of fringes (i.e. larger deflection) at the same input voltage. For instance, an input voltage of 10V applied to arms 2 and 3 resulted in an upward out-of-plane deflection of approximately 10.5 µm for the microactuator fabricated without the Poly0 layer compared to approximately 13.3 µm for the one fabricated with the Poly0 layer. As mentioned before, to obtain a downward out-of-plane deflection, the voltage is applied to the contact pads corresponding to the microactuator arms 1 and 4. Although the direction of the deflection was verified successful, the fact that the air gap between the actuator and the silicon nitride layer is only 2 µm made it difficult to measure experimentally the full-range of operation of the microactuator in this mode of actuation. However, the analytical models and finite element simulations predict similar behavior to the ones showed for the upward motion for both types of microactuators.

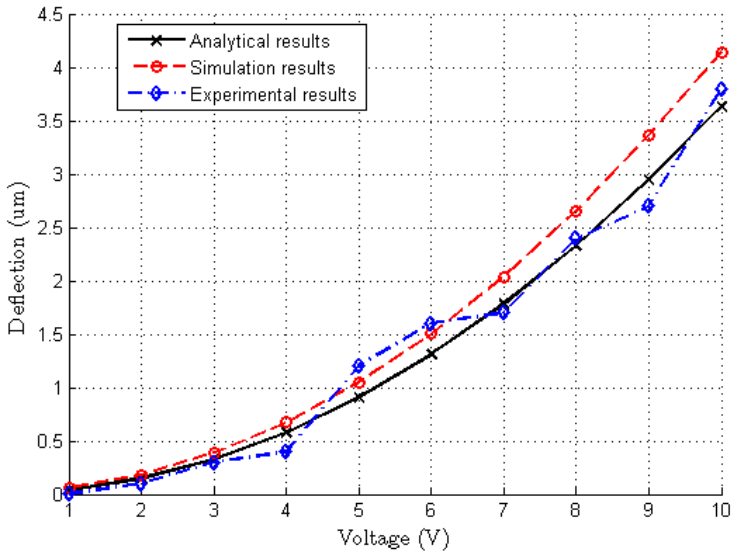

Figure 10. Experimental results compared to the analytical model and FEM simulations for a 2-DOF bidirectional microactuator fabricated with a Poly0 layer during in-plane motion (towards the right).

The comparison of the analytical model, simulations and experimental results for both the in-plane and out-of-plane deflection modes for the 2-DOF bidirectional microactuator fabricated with a Poly0 layer are shown in figures 10 and 11, respectively. It can be observed that for both of these modes, the experimental results match the analytical model and simulations closely. From these figures, it can be noticed that due to the limitations of the PolyMUMPs® process, the microactuators are more rigid in the horizontal direction, resulting in less in-plane deflections (3.7 µm at 10 V) compared to out-of-plane deflections (13.3 µm at 10 V). Hence, by designing and performing a custom fabrication process, both in-plane and out-of-plane deflections can be increased significantly. However, the complexity and cost of the fabrication will increase as well.

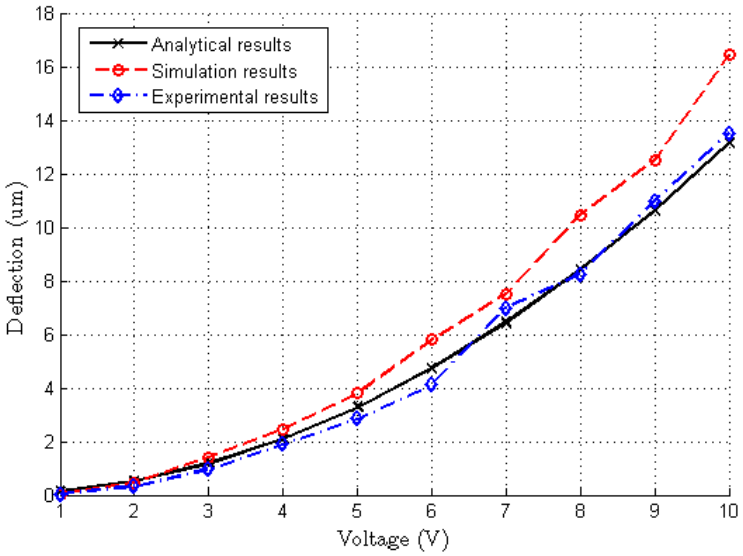

Figure 11. Experimental results compared to the analytical model and FEM simulations for a 2-DOF bidirectional microactuator fabricated with a Poly0 layer during out-of-plane motion (upward)

5. CONCLUSIONS

This paper introduced a 2-DOF bidirectional microactuator that operates purely by electrothermal actuation. A four-arm design is proposed to achieve the desired 2-DOF bidirectional motion. Two types of microactuators were fabricated which vary depending on the height between their inner and outer arms. The direction of motion was controlled by selectively applying voltage to different pairs of the four arms. The analytical solution of the deflection equation provides an insight about the operation of the device. Finite element model simulations were used to validate the analytical model with experimental results matching them very closely. The microactuators were fabricated using PolyMUMPs® and experimental results show that this foundry process gives enough flexibility to control the performance of the microactuators in the four directions. In-plane deflections of up to 3.7 µm were measured for an input voltage of 10 V. At this same input voltage and for the case of the out-of-plane motion, deflections of approximately 13.3 µm (upward) were measured. These values are comparable with state-of-the-art electrothermal actuators.

REFERENCES

[1] H. Guckel, J. Klein, T. Christenson, K. Skrobis, M. Laudon and E. G. Lovell "Thermo-magnetic metal flexure actuators," IEEE Solid-State Sensor and Actuator Workshop, 73-75 (1992)

[2] D. M. Burns and V. M. Bright, "Design and performance of a double hot arm polysilicon thermal actuator," Proc. SPIE Int. Soc. Opt. Eng., 296-306 (1997)

[3] C. H. Comtois, V. M. Bright and M. W. Phipps, 1995 "Thermal microactuators for surface-micromachining processes," Proc SPIE Int. Soc. Opt. Eng., 10-21 (1995)

[4] S. Deladi, G. Krijnen and M. C. Elwenspoek, "Parallel-beams/lever electrothermal out-of-plane actuator," Microsyst. Technol. 10, 393-399 (2004)

[5] R. Venditti, J. S. H. Lee, Y. Sun and D. Li, "An in-plane, bi-directional electrothermal MEMS actuator," J. Micromech. and Microeng. 16, 2067-2070 (2006).

[6] A. Cao, J. Kim and L. Lin, “Bi-directional electrothermal electromagnetic actuators," J. Micromech. and Microeng. 17, 975-982 (2007).
[7] K. M. Liao, C. C. Chueh and R. Chen, "A novel electro-thermally driven bi-directional microactuator," Proc 2002 Intal Symp on Micromechatronics and Human Science, 267-274 (2002).
[8] C. T. Wu and W. Hsu, "An electro-thermally driven microactuator with two dimensional motion," Microsyst. Technol. 8, 47-50 (2002).
[9] L. Lin and M. Chiao, “Electrothermal responses of lineshape microstructures,” Sensors and Actuators A, A55, 35-41(1996).
[10] D. G. Elms, “Linear Elastic Analysis,” B. T. Batsford Ltd, London, 38 (1970).
[11] J. Carter, A. Cowen, B. Hardy, R. Mahadevan, M. Stonefield and S. Wilcenski, “POLYMUMPS design handbook revision,” v11.0 http://www.memscap.com/mumps/documents/PolyMUMPs.DR.v11.pdf, MEMSCAP Inc, (2005).